NEUROPHYSIOLOGY

The mammalian circadian pacemaker regulates wakefulness via CRF neurons in the paraventricular nucleus of the hypothalamus

Daisuke Ono[1,2,3]*, Yasutaka Mukai[1,2,3,4], Chi Jung Hung[1,2,3,4], Srikanta Chowdhury[1,2,3†], Takashi Sugiyama[5], Akihiro Yamanaka[1,2,3]*

In mammals, the daily rhythms of physiological functions are timed by the central circadian clock located in the suprachiasmatic nucleus (SCN) of the hypothalamus. Although the importance of the SCN for the regulation of sleep/wakefulness has been suggested, little is known about the neuronal projections from the SCN, which regulate sleep/wakefulness. Here, we show that corticotropin-releasing factor (CRF) neurons in the hypothalamic paraventricular nucleus mediate circadian rhythms in the SCN and regulate wakefulness. Optogenetic activation of CRF neurons promoted wakefulness through orexin/hypocretin neurons in the lateral hypothalamus. In vivo Ca^{2+} recording showed that CRF neurons were active at the initiation of wakefulness. Furthermore, chemogenetic suppression and ablation of CRF neurons decreased locomotor activity and time in wakefulness. Last, a combination of optical manipulation and Ca^{2+} imaging revealed that neuronal activity of CRF neurons was negatively regulated by GABAergic neurons in the SCN. Our findings provide notable insights into circadian regulation of sleep/wakefulness in mammals.

INTRODUCTION

Living organisms exhibit endogenous circadian rhythms and adapt to the 24-hour daily cycle on earth. Circadian rhythms are known to organize the temporal timing of physiology and behavior such as of body temperature, metabolism, and sleep/wakefulness (*1*). In mammals, the suprachiasmatic nucleus (SCN) of the hypothalamus functions as the master circadian pacemaker; it is composed of thousands of neurons that express self-sustained and synchronized circadian rhythms in their electrical activity and gene expression (*2*, *3*). In individual SCN cells, a transcription-translation negative feedback loop is responsible for circadian oscillations. Briefly, the BMAL1/CLOCK heterodimers activate the transcription of the *Per* and *Cry* genes; in turn, the protein products of these genes suppress their own transactivation (*4*).

The SCN receives local light input from the retina (*5*), and the circadian rhythms of the SCN entrain to the environmental light-dark (LD) cycles. The SCN, in turn, regulates the timing of sleep and wakefulness. Electrical lesioning of the SCN results in deterioration of circadian behavioral rhythms (*6*). Neuronal outputs of the SCN are considered crucial in organizing the rhythms of sleep and wakefulness, for when neuronal projections from the SCN are cut with a Halasz knife (to create a hypothalamic "island" containing the SCN), firing rhythms are preserved within the island, but its rhythms outside the island and circadian behavior deteriorated (*7*). Almost all SCN neurons are γ-aminobutyric acid (GABA)–producing neurons (*8*), and the SCN-specific depletion of GABA function results in deterioration of circadian behavioral rhythms, indicating that GABAergic outputs are important for circadian behavior (*9*).

Sleep and wakefulness are regulated by several neuronal populations. Classically, the preoptic area (POA) and the posterior hypothalamus are thought to be the sleep and wake centers, respectively. However, recent studies have revealed new brain areas and neurons involved in the regulation of sleep/wakefulness. For instance, adenosine A_{2A}–expressing neurons in the nucleus accumbens are involved in the regulation of nonrapid eye movement (NREM) sleep (*10*). GABAergic neurons in the medullary parafacial zone located in the brain stem and the ventral tegmental area are also involved in the regulation of NREM sleep (*11*, *12*). The POA contains not only sleep-promoting neurons but also wake-promoting neurons (*13*). In contrast, noradrenergic neurons in the locus coeruleus, serotonergic neurons in the dorsal raphe, and histaminergic neurons in the tuberomammillary nucleus (TMN) are implicated in regulation of wakefulness (*14*). Orexin/hypocretin neurons in the lateral hypothalamus (LH) are thought to play a crucial role to maintain wakefulness by orchestrating the activity of these monoaminergic neurons (*15*, *16*). Although several efferent brain areas of the SCN are suggested, including the ventrolateral POA, dorsomedial hypothalamus, and subparaventricular zone (*17*–*19*), it still remains unclear which neuronal pathways are crucial for the circadian regulation of sleep/wakefulness. In the present study, we found that the SCN neurons negatively regulate activity in the corticotropin-releasing factor (CRF) neurons in the paraventricular nucleus (PVN) of the hypothalamus; in turn, CRF neurons positively regulate orexin neurons, which promote wakefulness. These results suggest that this neural pathway is crucial for circadian regulation of sleep and wakefulness in mammals.

RESULTS

Optogenetic activation of CRF neurons in the PVN promotes wakefulness

To identify the neuronal pathways from the SCN that are involved in the regulation of sleep and wakefulness, we first performed anterograde tracing of SCN neurons by injection of adeno-associated

[1]Department of Neuroscience II, Research Institute of Environmental Medicine, Nagoya University, Furo-cho, Chikusa-ku, Nagoya 464-8601, Japan. [2]Department of Neural Regulation, Nagoya University Graduate School of Medicine, Nagoya 466-8550, Japan. [3]CREST, JST, Honcho Kawaguchi, Saitama 332-0012, Japan. [4]JSPS Research Fellowship for Young Scientists, Tokyo 102-0083, Japan. [5]R&D, Olympus Corporation, Tokyo, Japan.
*Corresponding author. Email: dai-ono@riem.nagoya-u.ac.jp (D.O.); yamank@riem.nagoya-u.ac.jp (A.Y.)
†Present address: Department of Biochemistry and Molecular Biology, University of Chittagong, Chittagong-4331, Bangladesh.

virus (AAV) with Cre-dependent expression of humanized renilla green fluorescent protein (hrGFP) into the SCN (Fig. 1A). We used glutamic acid decarboxylase (GAD) 67–Cre mice because almost all SCN neurons are GABAergic (*8*). Histochemical examination revealed that axons of the SCN neurons were observed in several brain areas (Fig. 1B). They were densely observed in the PVN of the hypothalamus.

Several types of neurons are located in the PVN (*20*). Among them, CRF neurons have been importantly implicated in the stress response (*21*). As stress causes hyperarousal, we hypothesized that CRF neurons in the PVN are involved in the regulation of sleep/wakefulness. To test this, we injected AAV with Cre-dependent expression of channelrhodopsin-2 (E123T/T159C) fused with enhanced yellow fluorescent protein (AAV-CMV-flex-ChR2-EYFP) or hrGFP (AAV-CMV-flex-hrGFP, control) into the PVN of CRF-Cre mice and then implanted an optical fiber with electroencephalography (EEG) and electromyography (EMG) electrodes (Fig. 1, C and D, and fig. S1, A and B). In brain slices, we confirmed that blue light induced action potentials in the ChR2-expressed CRF neurons in the PVN with more than 90% firing fidelity (fig. S1, C to F). To control neuronal activity in vivo, we optogenetically activated CRF neurons in the PVN (10 Hz, 30 s). Wakefulness, NREM, and REM sleep were classified on the basis of EEG and EMG recordings (*22*). Activation of CRF neurons in the PVN increased the probability of wakefulness and reduced the probability of NREM and REM sleep (Fig. 1, E to G). The effect was evident in the dark period [zeitgeber times (ZT) 12 to 17 and ZT18 to 23, where ZT0 and 12 are lights on and off, respectively] and the latter half of the light period (ZT6 to 11) but was attenuated at the beginning of the light period (ZT0 to 5) (Fig. 1, F and G). Blue light–induced wakefulness was not observed in the control mice (fig. S1, H to K). Together, these results suggest that activation of CRF neurons in the PVN induces wakefulness.

Projection of CRF neurons in the PVN to orexin neurons in the LH promotes wakefulness

Next, to identify the downstream brain regions of CRF neurons in the PVN that regulate wakefulness, we injected AAV with Cre-dependent expression of hrGFP into the PVN of CRF-Cre mice and observed the localization of these axons within several brain areas (fig. S2, A to C). Among them, we focused on the LH because immunohistochemical analysis revealed that axons of CRF neurons in the PVN were evident near the orexin neurons in the LH (Fig. 2, A and B). We hypothesized that CRF neurons in the PVN regulate wakefulness via activation of orexin neurons in the LH, as it is known that orexin neurons are important for maintenance of wakefulness (*23*).

To determine whether the neuronal pathway from CRF neurons in the PVN to the LH regulates wakefulness, we injected AAV-CMV-flex-ChR2-EYFP into the PVN of CRF-Cre mice and placed optical fibers into the LH (Fig. 2, C and D). We found that optogenetic activation of nerve terminals of CRF neurons at the LH promoted wakefulness (Fig. 2, E to G), similar to the result of cell body stimulation (Fig. 1). Blue light–induced wakefulness was not observed in the control mice (fig. S2, D to G). These results suggest that the neuronal pathway from CRF neurons in the PVN to the LH is critical for induction of wakefulness.

Moreover, to examine whether activity of CRF neurons in the PVN activates the orexin neurons in the LH, we applied optogenetics to activate the nerve terminals of CRF neurons of the PVN into the LH using brain slices and then electrophysiologically measured firing from the orexin neurons. To achieve precise control of gene expression in different types of neurons in the hypothalamus, we generated CRF-Cre;orexin flippase (Flp) bigenic mice in which the CRF neurons and orexin neurons exclusively express Cre recombinase and Flp recombinase, respectively (*24*). We subsequently injected AAV into the brain to express ChR2-EYFP and tdTomato in the CRF neurons and orexin neurons, respectively (Fig. 2, H and I). As we expected, blue light increased the firing frequency of some orexin neurons (21.7%; 5 of 23 neurons) (Fig. 2, J and K). Recently, rabies virus–mediated monosynaptic retrograde tracing of orexin neurons revealed that CRF neurons in the PVN have direct input to orexin neurons in the LH (*25*). Together, these results suggest that activation of CRF neurons in the PVN activates orexin neurons in the LH.

CRF neurons in the PVN facilitate wakefulness

As CRF neurons in the PVN were shown to promote wakefulness (Fig. 1), we assumed that CRF neurons were active during wakefulness. To test this, we used the in vivo fiber photometry method. We injected AAV with Cre-dependent expression of the genetically encoded Ca^{2+} indicator, G-CaMP6 (*26*), into the PVN of CRF-Cre mice (Fig. 3, A and B). We collected G-CaMP6 fluorescence through an optical fiber placed above the PVN. First, we confirmed that the tail suspension (physical stress) increased Ca^{2+} signals in the CRF neurons (fig. S1, A and B), indicating that these neurons respond to external physical stress (*27*). Next, we recorded Ca^{2+} signals from the CRF neurons, together with EEG and EMG recordings. As we expected, Ca^{2+} signals in the CRF neurons were high during wakefulness but low during NREM and REM sleep (Fig. 3, C to E, and fig. S3). We also found that the intensity of the calcium signal from the CRF neurons in the PVN gradually decreased during wakefulness (fig. S3D). These results suggest that CRF neurons in the PVN facilitate wakefulness.

Chemogenetic suppression and ablation of CRF neurons in the PVN attenuate wakefulness and locomotor activity

If the CRF neurons in the PVN are crucial for wakefulness, then suppression of neuronal activity of these neurons should attenuate wakefulness. To assess this possibility, we tested the effects of chemogenetic suppression of CRF neurons in the PVN on sleep and wakefulness. For the suppression experiment, we injected AAV-CAG-flex-hM4Di-mCherry into the PVN of CRF-Cre mice (Fig. 4, A to C). Compared with vehicle injection, clozapine-*N*-oxide (CNO) injection significantly suppressed time in wakefulness and increased time in NREM sleep (Fig. 4, D and E, and fig. S4A).

We subsequently further examined the role of CRF neurons in the PVN in controlling circadian-regulated wakefulness. Therefore, we injected AAV with Cre-dependent expression of diphtheria toxin A (DTA) (AAV-CMV-flex-mCherry/DTA) into the PVN to induce specific ablation of CRF neurons (Fig. 4F). CRF neurons in the PVN were partially ablated (50 to 60%) by DTA expression (Fig. 4, G and H). We measured locomotor activity using an infrared sensor, as previously reported (Fig. 4I and fig. S4B) (*28*). Four weeks after AAV injection, mice were transferred from their LD cycle to constant darkness (DD). The daily pattern of locomotor activity was different between CRF-DTA and control mice under LD at 4 weeks

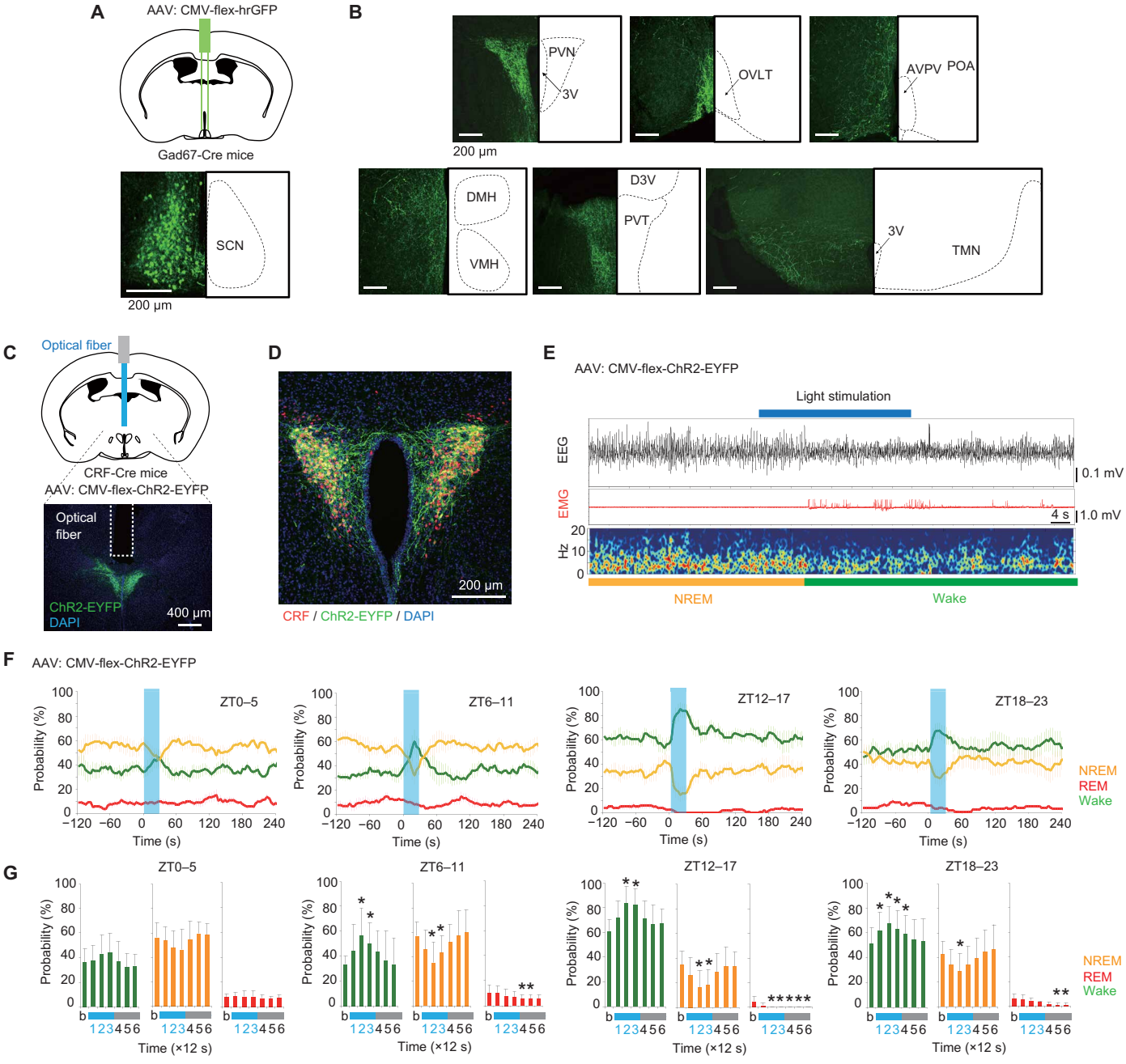

Fig. 1. Optogenetic stimulation of the CRF neurons in the PVN promotes wakefulness. (**A**) Schematic drawing of anterograde tracing experiment (top) and fluorescence image of the SCN in a GAD67-Cre mouse injected with AAV-CMV-flex-hrGFP (bottom). (**B**) Fluorescence images of several brain areas in a GAD67-Cre mouse with AAV-CMV-flex-hrGFP injected into the SCN. (**C**) Schematic drawing of optogenetic activation experiment in vivo and fluorescence image of the PVN in a CRF-Cre mouse injected with AAV-CMV-flex-ChR2-EYFP. (**D**) A fluorescence image of ChR2-EYFP (green), CRF (red), and DAPI (4′,6-diamidino-2-phenylindole) (blue) of the PVN in a CRF-Cre mouse. (**E**) A representative example of the electroencephalography (EEG) and electromyography (EMG) traces, together with the EEG power spectrum. The blue bar indicates light stimulation (10 Hz for 30 s). (**F**) Probability of wakefulness and NREM and REM sleep before, during, and after blue light stimulation (mean ± SD). Blue shading areas indicate light flashing. (**G**) Statistical results of the probability of a vigilant state before (indicated as "b"), during, and after blue light stimulation. The mean probability during 12 s (three epochs) obtained from (F) is shown in the bar graphs (mean ± SD; $n = 5$). Blue characters (1 to 3) indicate during stimulation (*$P < 0.05$ versus baseline; one-way repeated-measures analysis of variance with post hoc Tukey-Kramer test, or Friedman test with post hoc Steel-Dwass test). PVT, paraventricular thalamus; OVLT, organum vasculosum laminae terminalis; AVPV, anteroventral periventricular nucleus; VMH, ventromedial hypothalamus; D3V, dorsal part of the third ventricle.

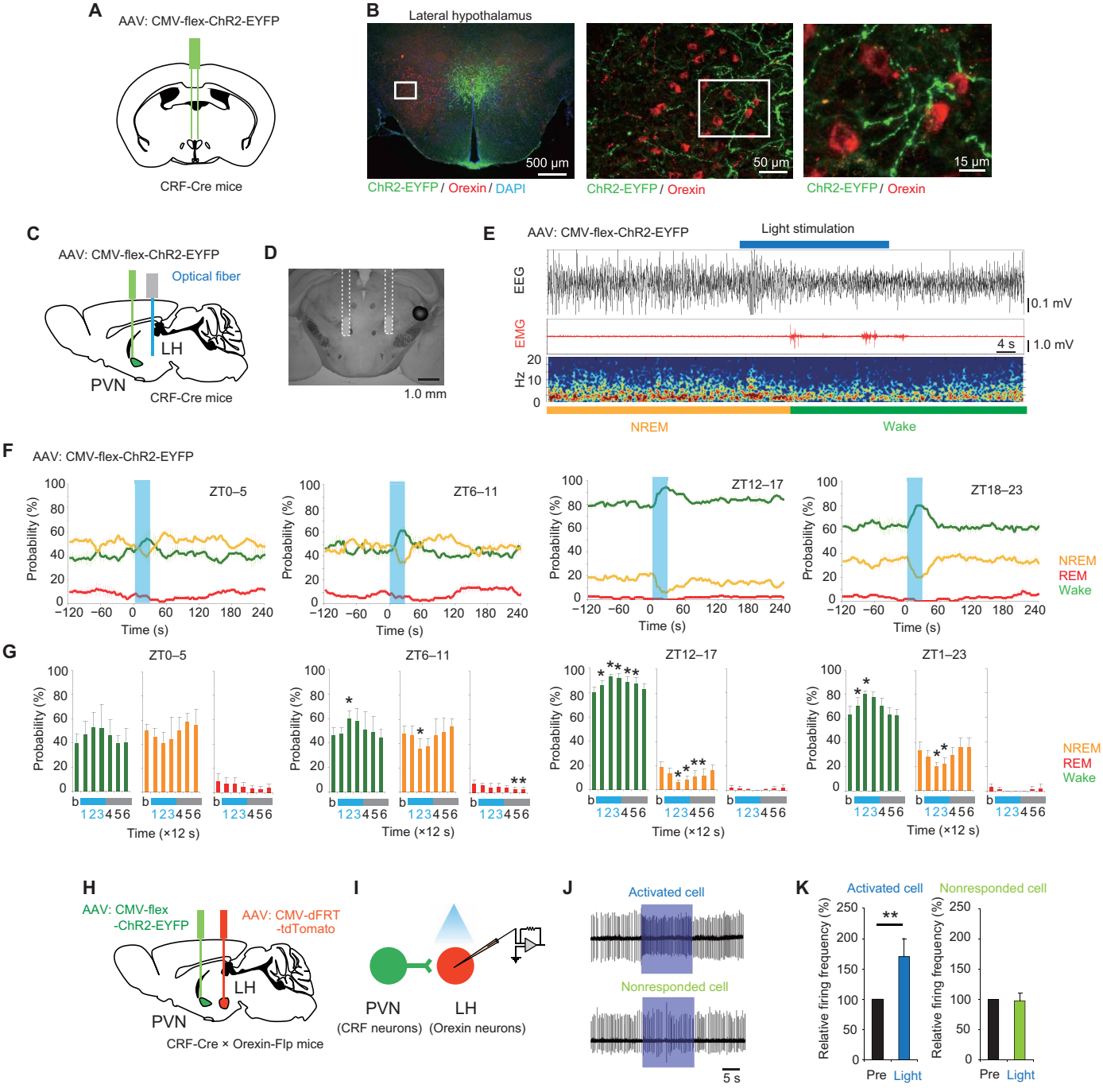

Fig. 2. Projection of CRF neurons in the PVN to orexin neurons in the LH promotes wakefulness. (**A** and **B**) Schematic drawing of anterograde tracing of CRF neurons in the PVN (A) and fluorescence images of the LH (B). Green and red indicate CRF neurons in the PVN and orexin neurons in the LH, respectively. (**C** and **D**) Schematic drawing of optogenetic stimulation of nerve terminals of CRF neurons of the PVN at the LH in vivo (C) and bright-field image of brain slice (D). (**E**) A representative example of EEG and EMG traces, together with the EEG power spectra. The blue bar indicates light stimulation (10 Hz for 30 s). (**F**) Probability of wakefulness and NREM and REM sleep before, during, and after blue light stimulation (mean ± SD). Blue shading areas indicate light flashing. (**G**) Statistical results of the probability of a vigilant state before (indicated as "b"), during, and after blue light stimulation. The mean probability during three epochs (12 s) obtained from (F) is shown in the bar graphs (mean ± SD; $n = 5$). Blue characters (1 to 3) indicate during stimulation (*$P < 0.05$ versus baseline; one-way repeated-measures analysis of variance with post hoc Tukey-Kramer test). (**H** and **I**) Schematic drawing of optogenetic stimulation of nerve terminals of CRF neurons of the PVN and electrophysiological recording from orexin neurons in the LH. (**J**) Representative traces of firing in a loose cell-attached mode recording from orexin neurons. Blue shading areas indicate continuous light illumination. When firing frequency during light illumination was increased more than 125% of basal level, these neuros were defined as activated neurons. (**K**) Normalized percentage of firing frequency before and during light stimulation. (**$P < 0.01$; one-sample t test).

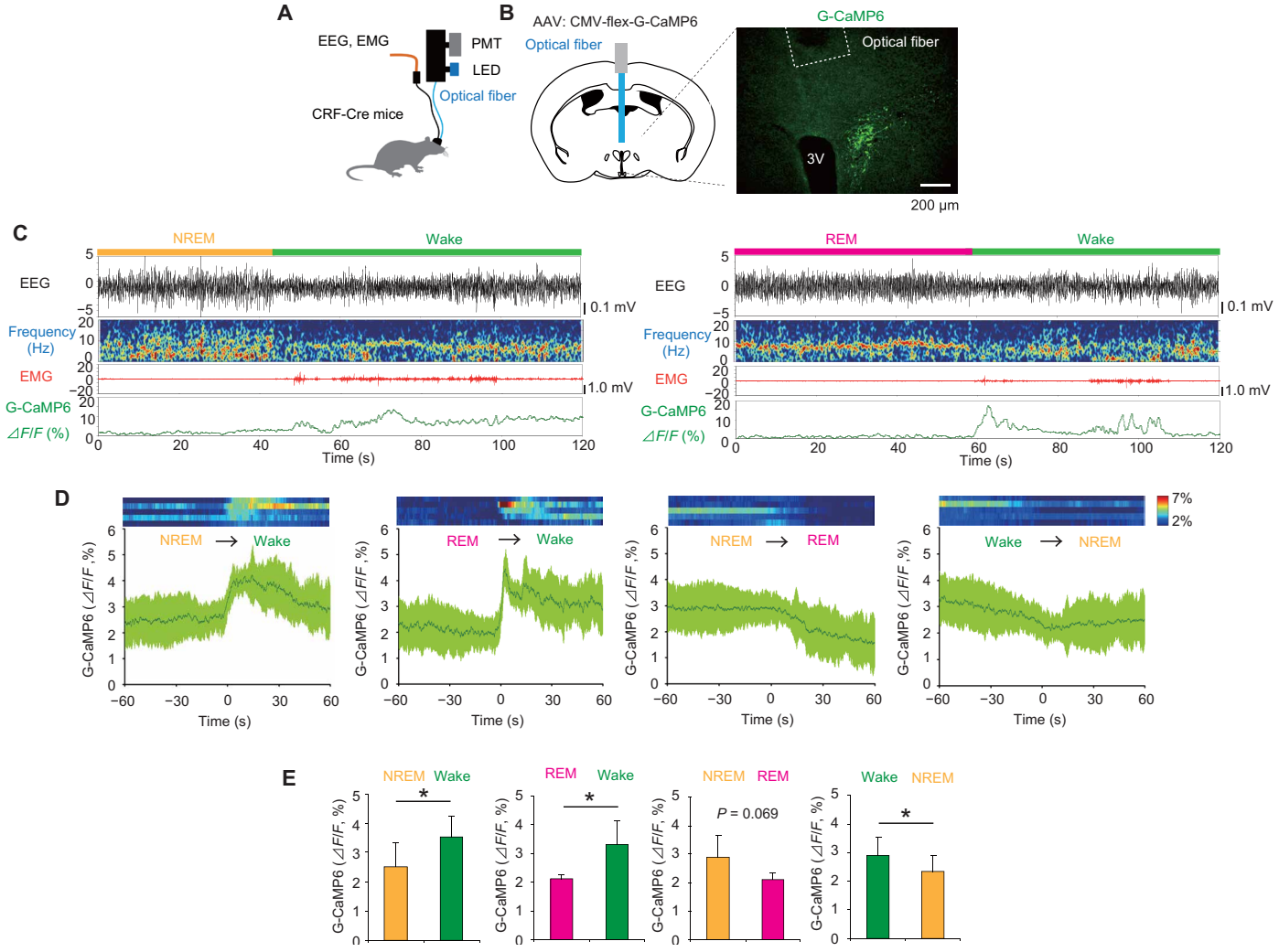

Fig. 3. CRF neurons in the PVN are preferentially active during wakefulness. (**A**) Schematic drawing of the setup of fiber photometry system. (**B**) Schematic drawing of optical recording from the CRF neurons in the PVN and a fluorescence image of G-CaMP6 expressing CRF neurons. (**C**) Representative examples of the EEG, EEG power spectrum, EMG, and G-CaMP6 signals in the CRF neurons. (**D**) Changes in G-CaMP6 signals before and after each vigilance state transition. Heatmaps indicate mean G-CaMP6 signal changes (Δ*F*/*F*, %) in individual animals (mean ± SD; $n = 5$). Green lines indicate mean signals from all animals. Shaded green areas indicate SD. (**E**) Statistical results of G-CaMP6 signals in the transition of each vigilance state (area under the curve during 60 s before and after tradition) (mean ± SD; $n = 5$; $^*P < 0.05$; paired *t* test or Wilcoxon signed-rank test).

(Fig. 4K and fig. S4C) and significantly different between the two groups especially at the beginning of the active phase during DD (subjective night) (Fig. 4L and fig. S4C). The free-running period of behavioral rhythms did not differ between the two groups (Fig. 4J). Attenuated locomotor activity in CRF-DTA mice could reflect reduction of active wakefulness. These results further support the functional importance of CRF neurons in the PVN for the circadian regulation of wakefulness.

GABAergic neurons in the SCN regulate the neuronal activity of CRF neurons in the PVN

Since axons of GABAergic neurons in the SCN were densely observed in the PVN (Fig. 1), we wondered whether the neuronal activity of CRF neurons in the PVN is regulated by the SCN. To address this, we performed Ca^{2+} imaging from brain slices including both the SCN and PVN. We prepared a brain slice containing both the SCN and PVN areas from bigenic mice (CRF-Cre/Rosa 26-LSL-tdTomato mice) in which CRF neurons exclusively express tdTomato. We observed tdTomato-expressed neurons in the PVN area in the brain slice, indicating that CRF neurons were present in the slice (Fig. 5A). We also applied AAV-hSyn-GCaMP6s into the brain slice to monitor intracellular Ca^{2+} concentration from the SCN and PVN neurons. Then, we performed time-lapse imaging (1-hour interval) and observed clear circadian Ca^{2+} rhythms, with the sinusoidal-like shape, in the SCN (Fig. 5, B and C). We observed calcium spikes in the PVN around the trough phase of SCN Ca^{2+} rhythms (Fig. 5C). As the phase relationship between the SCN and PVN areas appeared to be in antiphase (Fig. 5C), we measured Ca^{2+} intensity at a higher time resolution (1-s interval) during both subjective day and night (Fig. 5D). Intracellular Ca^{2+} concentration in the SCN was high in the subjective day and low in the subjective night, whereas in the PVN, it was high in the

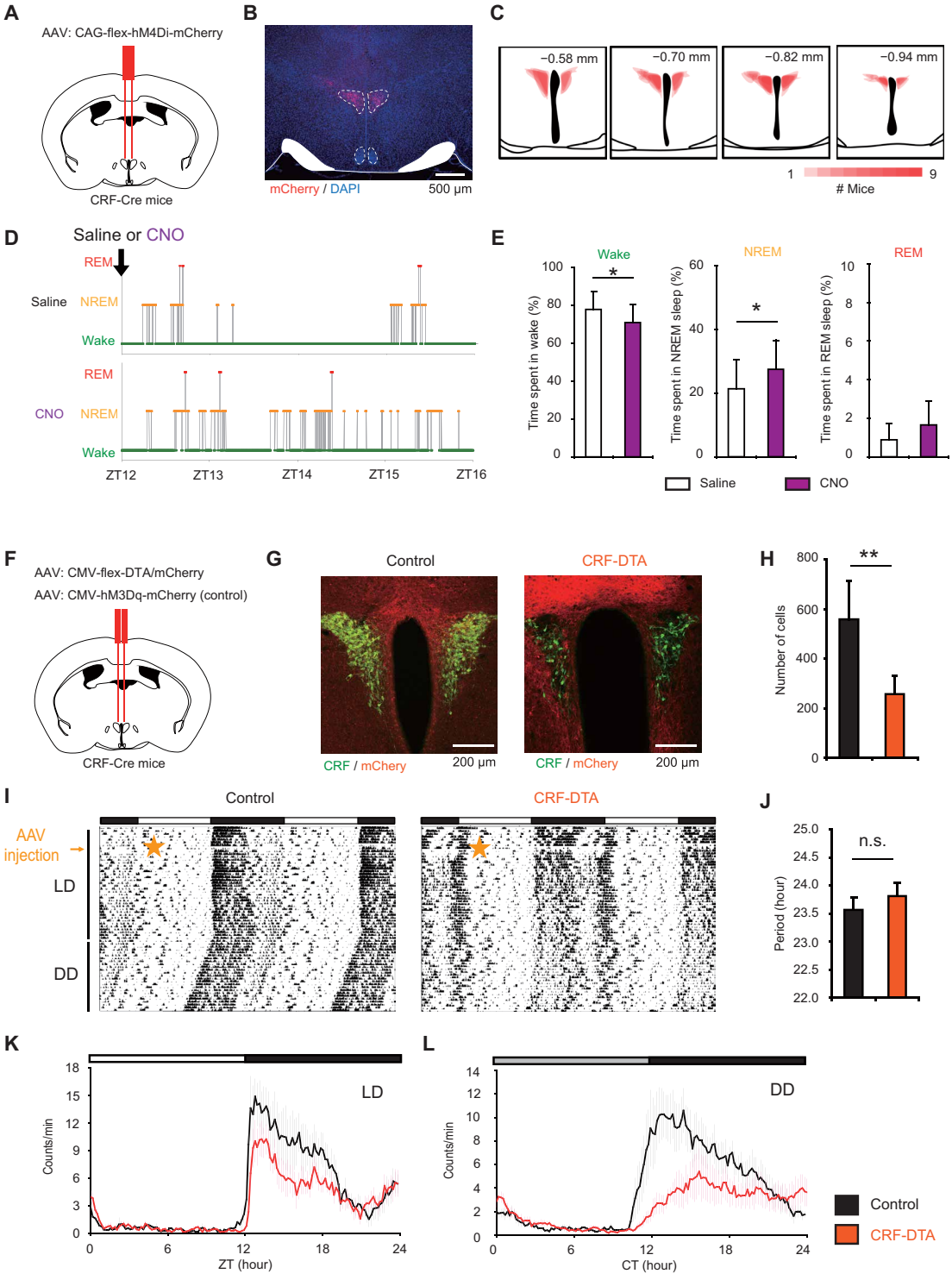

Fig. 4. Chemogenetic suppression and ablation of CRF neurons in the PVN attenuate wakefulness and locomotor activity. (**A**) Schematic drawing of the chemogenetic experiment. (**B**) A fluorescence image of the PVN in a CRF-Cre mouse with AAV-CAG-flex-hM4Di-mCherry injected into the PVN. (**C**) Histological verification and reconstruction of hM4Di-mCherry–expressing areas in the PVN. (**D**) Representative hypnograms during 4 hours after saline or CNO (1 mg/kg of body weight) injection in a CRF-Cre mouse expressing hM4Di-mCherry in CRF neurons of the PVN. (**E**) Percentage of time spent in each state during the 2 hours after injection (means ± SD; **P* < 0.05; Wilcoxon signed-rank test; *n* = 9). (**F**) Schematic drawing of the CRF neuron ablation experiment. (**G**) Fluorescence images of the PVN in a CRF-Cre mouse with AAV-CMV-flex-DTA/mCherry or AAV-CMV-hM3Dq-mCherry (control). (**H**) Number of CRF neurons in the PVN from CRF neurons ablated (CRF-DTA) and control mice (***P* < 0.01; Student's *t* test). (**I**) Representative actograms of locomotor activity from CRF–diphtheria toxin A (DTA) and control mice. Orange stars indicate the timing of AAV injection. (**J**) Mean free-running period under constant darkness (DD). n.s., not significant. (**K** and **L**) Daily profiles of circadian behavioral rhythms under LD (K) and DD (L). Activity counts of control (black; *n* = 5) and CRF-DTA (red; *n* = 7) mice were plotted every 10 min. Data are shown as means ± SD.

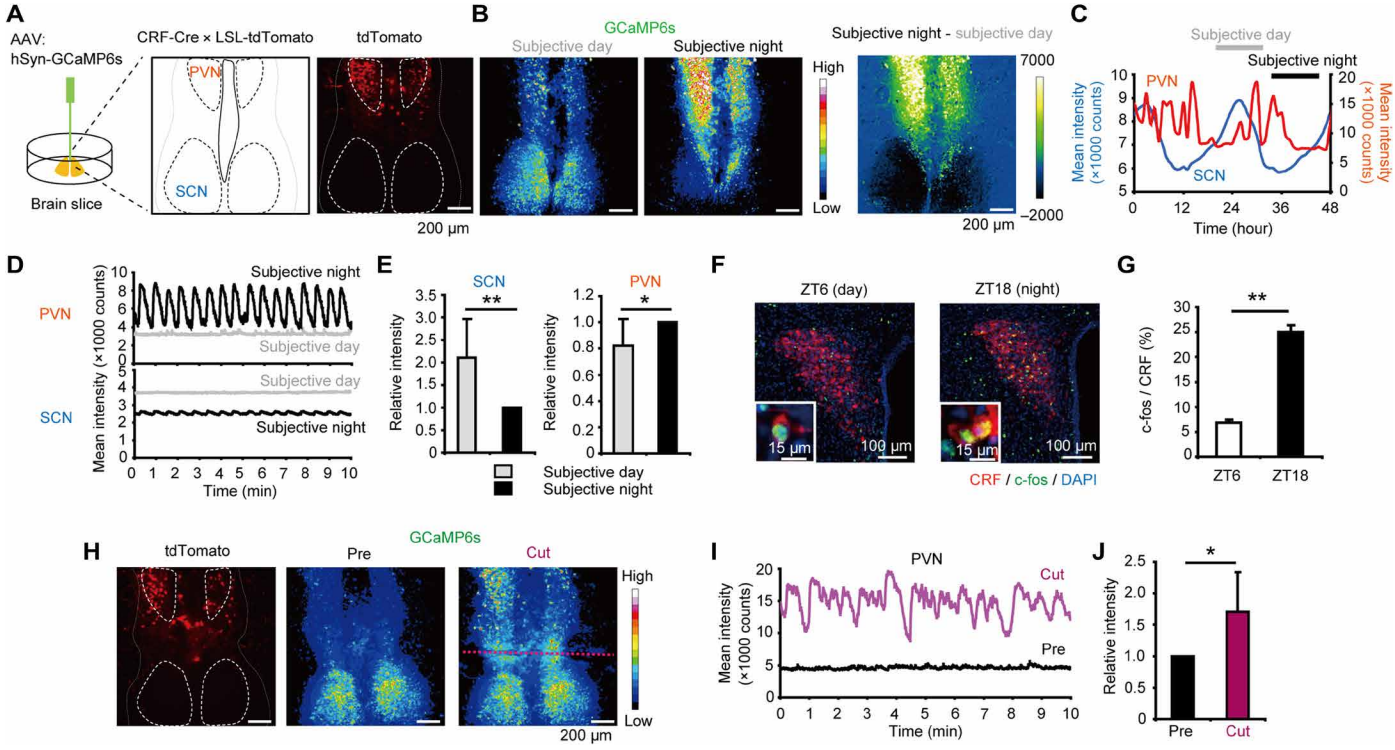

Fig. 5. The neuronal activity of CRF neurons in the PVN is regulated by the SCN. (**A**) Schematic drawing of the calcium imaging experiment from the SCN and PVN brain slice and a fluorescence image of tdTomato expressed in the CRF neurons. (**B**) Mean intensity of GCaMP6s during subjective day and night (left) and a color map of GCaMP6s data subtracted from subjective day to night (right). (**C**) GCaMP6s signal changes in the SCN (blue) and PVN (red) during 48 hours. Data were obtained every 1 hour. (**D**) GCaMP6s signal changes in the SCN and PVN during subjective day (gray) and night (black). Data were obtained every 1 s. (**E**) Quantified results of GCaMP6s intensity in the SCN and PVN during subjective day and night. (**$P < 0.01$ and *$P < 0.05$; paired *t* test; $n = 10$). (**F**) Fluorescence immunostaining of CRF and c-Fos of the PVN during the day (ZT6) and night (ZT18). (**G**) Percentage of c-Fos–positive neurons in the CRF neurons in the PVN during the day and night (**$P < 0.01$; Student's *t* test). (**H**) Fluorescence image of tdTomato expressed in the CRF neurons (left) and mean GCaMP6s intensity before (middle) and after knife cutting (right) between the SCN and PVN (purple dotted line). (**I**) GCaMP6s signal changes in the PVN before and after knife cutting. (**J**) Quantified data of the GCaMP6s signal before and after knife cutting. (*$P < 0.05$; paired *t* test; $n = 8$).

subjective night and low in the subjective day (Fig. 5, D and E, and fig. S5, A and B). Furthermore, calcium spikes were observed in the PVN especially in the subjective night (Fig. 5D and movie S1). We also measured c-Fos expression in the CRF neurons of the PVN in vivo using immunostaining and found that the expression rate was significantly high during the night (ZT18) compared to during the day (ZT6) (Fig. 5F). Overall, these results suggest that the neuronal activity of CRF neurons in the PVN could be regulated by the SCN.

To further elucidate how the SCN regulates neuronal activity of CRF neurons in the PVN, we physically separated the SCN and PVN areas in the brain slice by knife cutting and measured the Ca^{2+} signals (Fig. 5H). Ca^{2+} signals in the PVN were elevated after knife cutting of the slice, and calcium spikes were frequently observed in the PVN, which was a pattern similar to that observed during subjective night (Fig. 5, I and J; fig. S5, C and D; and movie S2). These results suggest that activity of SCN neurons negatively regulates the neuronal activity of CRF neurons in the PVN.

Next, we tested the function of SCN neurons in the PVN using optical imaging and optogenetics. We applied AAV-EF1a-flex–stabilized step function opsin (SSFO)–mCherry and AAV-hSyn-Okiluc-CaM (a split-type Ca^{2+} bioluminescence indicator; see Materials and Methods) into the SCN-PVN brain slice from Gad67-Cre or vesicular GABA transporter (VGAT)–IRES-Cre mice (Fig. 6A and fig. S5G). That is, GABAergic neurons expressed SSFO and all neurons in the slice expressed Okiluc-CaM. A decrease in bioluminescence intensity from Okiluc-CaM reflected an increase in the intracellular Ca^{2+} (fig. S5, E and F). Optogenetic activation (470 nm) of GABAergic neurons in the SCN increased the Ca^{2+} level, indicating that SCN neurons were activated by light. Conversely, the Ca^{2+} level in the PVN was suppressed by optogenetic activation of SCN neurons (Fig. 6B and fig. S5H). We further confirmed this interaction by using a different approach, where we infected AAV-CAG-flex-ChrimsonR-tdTomato and AAV-hSyn-GCaMP6s into SCN-PVN brain slices from VGAT-IRES-Cre mice to manipulate SCN neuronal activity and measured the Ca^{2+} signals in the SCN and PVN (Fig. 6C). Optogenetic activation (590 nm) of the GABAergic neurons in the SCN increased Ca^{2+} in the SCN but decreased Ca^{2+} in the PVN (Fig. 6, D to F; fig. S5, I to K; and movie S3). These results demonstrate that activation of SCN neurons suppresses neuronal activity in the PVN.

Since almost all SCN neurons are GABAergic (*8*), suppression of neuronal activity of PVN neurons by optogenetic activation of the SCN is likely mediated by GABA signaling. To further test this mechanism, we repeated the above experiment in the presence of the $GABA_A$ (GABA type A) receptor antagonist (gabazine) within the culture medium. Application of gabazine increased calcium

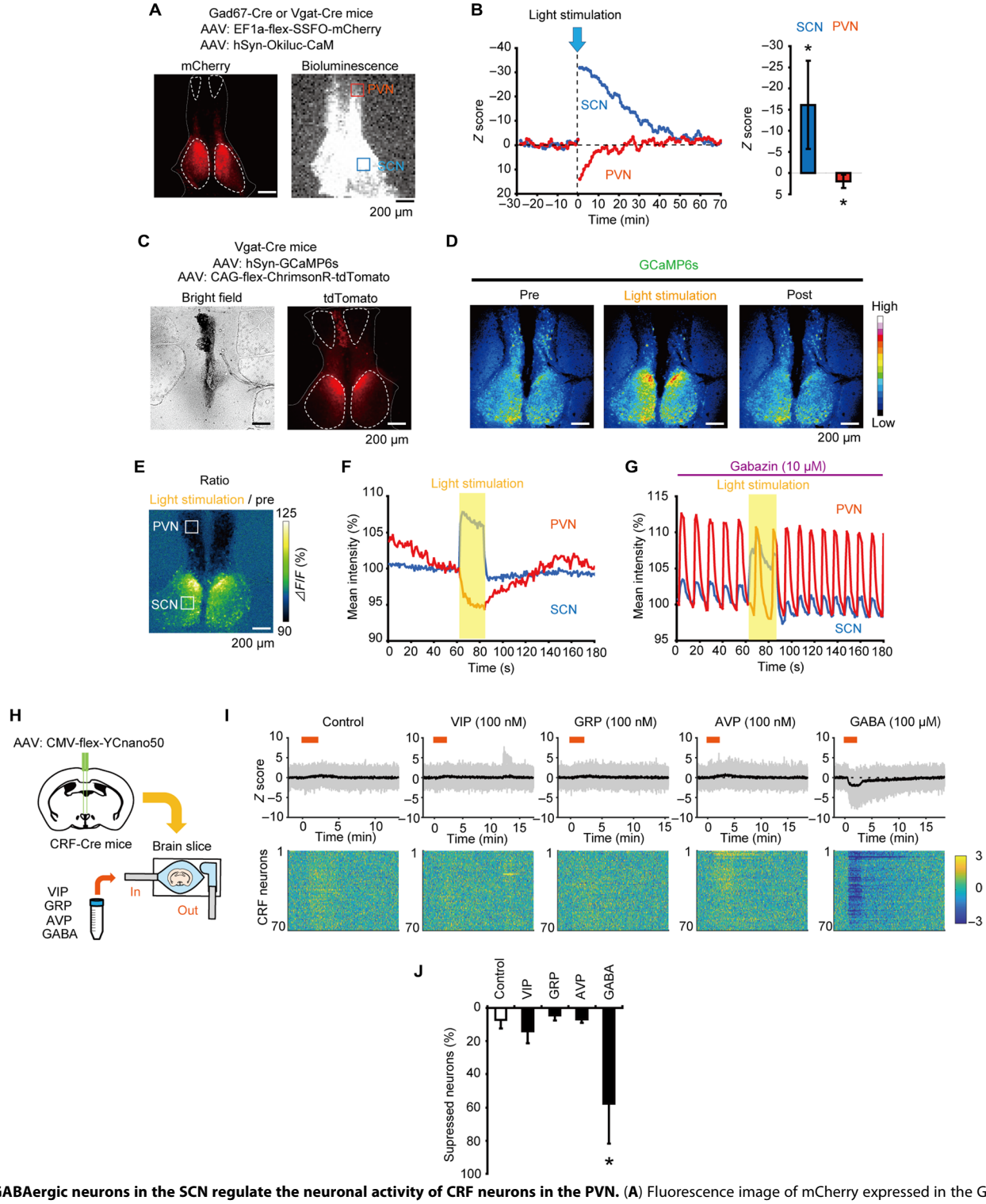

Fig. 6. GABAergic neurons in the SCN regulate the neuronal activity of CRF neurons in the PVN. (**A**) Fluorescence image of mCherry expressed in the GABAergic neurons in the SCN (left) and bioluminescence images. (**B**) Bioluminescence changes in the SCN (blue) and PVN (red). The blue arrow indicates the timing of blue light (488 nm) stimulation for 5 s. Bioluminescence intensity was expressed as the *Z* score. (*$P < 0.05$; paired *t* test; $n = 6$). (**C**) Bright-field and fluorescence images of a brain slice with ChrimsonR specifically expressed in the SCN. (**D**) Mean GCaMP6s intensity before (left), during (middle), and after (right) light stimulation. (**E**) A color map of GCaMP6s data expressed as $\Delta F/F$ obtained from before and during light stimulation. (**F**) Normalized GCaMP6s intensity from the SCN and PVN. The intensity of GCaMP6s before light stimulation is defined as 100. The yellow shaded area indicates yellow light (590 nm) stimulation. (**G**) Normalized GCaMP6s intensity from the SCN and PVN with $GABA_A$ receptor antagonist (gabazine) application. (**H**) Schematic drawing of the Ca^{2+} imaging from the CRF neurons in the PVN. (**I**) Representative examples of Ca^{2+} changes in CRF neurons in the PVN (top) and heatmap expressed by the *Z* score (bottom). (**J**) Percentage of CRF neurons whose Ca^{2+} was suppressed (*$P < 0.05$; Friedman test with post hoc Steel test; $n = 4$). Data are expressed as means ± SD.

spikes in the PVN, similar to the results of the physical separation (knife cut) experiment (Figs. 5, H and I, and 6G; and fig. S5L). Furthermore, optical activation of the SCN GABAergic neurons via ChrimsonR did not suppress the calcium spikes in the PVN within the presence of gabazine (Fig. 6G, fig. S5L, and movie S4). These results further support that GABA released from the SCN suppresses neuronal activity in the PVN.

Several types of neurons are distributed in the SCN such as vasoactive polypeptide (VIP), gastrin-releasing peptides (GRP), and arginine vasopressin (AVP)–expressing neurons, which are three major types of neurons in the SCN (*20*). To elucidate the direct effects of these peptide neurotransmitters on CRF neurons in the PVN, we performed Ca^{2+} imaging using the brain slices. We expressed the Förster resonance energy transfer–type Ca^{2+} indicator, yellow Cameleon-Nano50 (*29*), in the CRF neurons in the PVN by injecting AAV (Fig. 6H). Slices were prepared and perfused in artificial cerebrospinal fluid containing tetrodotoxin (TTX) to prevent synaptic interactions. Intracellular Ca^{2+} responses can then be monitored from the ratio of cyan fluorescent protein (CFP) and Venus fluorescence. VIP, GRP, or AVP application did not show clear effects, but GABA application markedly decreased intracellular Ca^{2+} in the PVN CRF neurons (Fig. 6, I and J). These results further confirm that GABA suppresses the excitability of CRF neurons in the PVN.

DISCUSSION

In this study, we identified a neuronal pathway originating from the SCN that is involved in the regulation of sleep and wakefulness. Optogenetics, together with optical imaging, revealed that the excitability of CRF neurons in the PVN is regulated by SCN GABAergic neurons. In vivo fiber photometry recordings further showed that CRF neurons facilitated wakefulness. Optogenetic activation of CRF neurons increased wakefulness, and this effect was at least partially regulated through the activation of orexin neurons in the LH. Chemogenetic suppression and DTA-mediated ablation of CRF neurons attenuated wakefulness and locomotor activity. These results strongly suggest that wakefulness is regulated via a SCN-PVN-LH pathway.

Environmental LD conditions change SCN neuronal networks (*30*), and circadian rhythms in the SCN could regulate multiple physiological functions via the PVN. For instance, the PVN neurons regulate melatonin release from the pineal gland (*31*), which is crucial for the regulation of photoperiodism such as reproductive function (*32*). In addition, the PVN is also known as an important nucleus for the tuning of body temperature, feeding behavior, and metabolism (*33*, *34*). CRF neurons in the PVN regulate blood corticosterone concentration, which is a critical factor for temporal regulation of the peripheral clock and stress response (hypothalamic-pituitary-adrenal axis) (*35*, *36*). Thus, CRF neurons in the PVN could work as an "interface" to transmit circadian information from the SCN to other brain areas and/or organs that temporally regulate physiological functions. It is also reported that CRF neurons in the PVN exhibited burst firings (*37*). In the present study, we observed calcium spikes in CRF neurons in the PVN, which was regulated by the GABAergic neurons in the SCN. These results suggest that CRF neurons in the PVN work as a "pulse generator" whose excitability is modulated by the SCN circadian oscillations.

We found that calcium signals in the CRF neurons in the PVN were increased at the initiation of wakefulness but gradually decreased afterward, even though mice were still awake (Fig. 3 and fig. S3). A similar characteristic was observed when aversive stimulation was applied (fig. S3) (*27*). These results suggest that the activation of CRF neurons facilitates the transition to wakefulness but may not be necessary to maintain later wakefulness. We also found that the activation of CRF neurons led to the subsequent activation of orexin neurons, which increased wakefulness. Furthermore, GABAergic neurons in the LH also have wake-promoting effects, which might be regulated by the CRF neurons in the PVN (*38*). Elevated intracerebroventricular CRF concentrations suppress the activity of GABAergic neurons in the POA and VLPO, which have a crucial role in the initiation and maintenance of NREM sleep (*39*). Therefore, both neural and humoral pathways might contribute to maintaining of wakefulness after transient activation of CRF neurons.

Our results showed that excitability of CRF neurons in the PVN is regulated by the SCN, which is crucial for the circadian regulation of wakefulness. On the other hand, CRF neurons are also involved in the stress response. For example, chemogenetic suppression of CRF neurons in the PVN attenuated acute stress–induced sleep disturbance (*40*). Circadian rhythms of sleep and wakefulness are regulated by the SCN, but when animals encounter severe life-threatening conditions, they need to keep awake to escape from danger even during inactive phases. Thus, the wake-promoting function of CRF neurons in the PVN might be regulated by both the circadian clock and stress responses that increase survival rate in nature.

We found that GABA release in the SCN decreased the intracellular Ca^{2+} concentration among PVN neurons, and GABA, not AVP, VIP, and GRP, application decreased Ca^{2+} among CRF neurons in the PVN under TTX treatment (Fig. 6). Together, these results suggest that GABAergic neurons in the SCN are crucial for excitability of CRF neurons in the PVN. It would be interesting to know whether this effect is due to direct pathways from the SCN to PVN neurons and which neuronal types within the SCN are involved. Further study is needed to elucidate this mechanism.

Previous studies have shown the possible downstream brain areas from the SCN (*18*–*20*, *41*–*43*). Although we identified one functional neuronal pathway that is involved in the regulation of wakefulness, our anterograde tracing of SCN neurons suggests that other downstream brain areas could also be involved in the regulation of sleep and wakefulness. Among them, the paraventricular thalamus (PVT) and TMN are known as crucial areas for wakefulness (*44*, *45*). In contrast, the POA is important for sleep (*13*, *46*). These pathways, together with the PVN to LH pathway, regulate the circadian regulation of sleep and wakefulness.

Before cloning of the clock gene, a two-oscillator model had been proposed to explain circadian behavior (*47*). In *Drosophila*, neuronal circuits that regulate activity onset and offset (morning and evening oscillators, respectively) have been identified (*48*). In the present study, the ablation of CRF neurons in the PVN attenuated the amount of locomotor activity especially in activity onset, and optogenetic activation of CRF neurons in the PVN promoted wakefulness especially at the beginning of the dark period. These results suggest that this pathway might be involved in the evening oscillator–related neuronal pathway from the SCN in mammals.

The electrical activity rhythm of the SCN, with a high day-time and low night-time firing rate, is the same in both nocturnal and diurnal animals (*7*, *49*). This suggests that diurnality/nocturnality is coded in the downstream neural pathway of the SCN. Our hypothetical model suggests that the SCN GABAergic neurons suppress

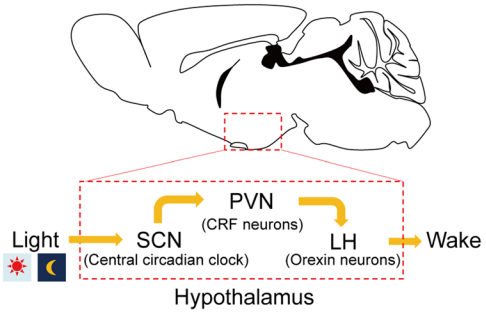

Fig. 7. A model of the central circadian clock regulation of wakefulness. Circadian rhythms in the SCN entrain to the environmental light and dark conditions through the retinohypothalamic tract. Inactivation of GABAergic neurons (subjective night) of the SCN increases CRF neuronal activity in the PVN, which could excite orexin neurons in the LH, thereby activating orexin neurons to control wakefulness. Activation of GABAergic neurons (subjective day) of the SCN decreases CRF neuronal activity in the PVN, which could suppress orexin neurons.

CRF neurons in the PVN, resulting in attenuation of wakefulness in nocturnal animals (Fig. 7). It is unclear how the nocturnal/diurnal behavior and physiological functions such as corticosterone release are regulated. However, because almost all SCN are GABAergic neurons and the excitability of GABA is modulated by intracellular Cl^- concentration depending on several factors (*50*), regulation of GABA excitability in the downstream brain areas including PVN and other brain areas might represent a potential mechanism, governing nocturnal versus diurnal behavior in mammals. Further research is required to fully understand this mechanism.

Sleep and wakefulness are regulated by both the circadian clock and homeostasis. The importance of the phosphorylation-dephosphorylation cycle among phosphoproteins for sleep-wake homeostasis has been recently suggested (*51*). In addition, a Ca^{2+}-dependent hyperpolarization pathway has also been proposed for the regulation of sleep in mammals (*52*). In the present study, we found a potential neuronal pathway that connects the SCN to sleep/wake regulation. The results suggest that circadian regulation of sleep and wakefulness is modulated by the SCN-PVN-LH pathway with other neuronal pathways. Since several sleep- or wake-promoting brain areas have been identified, it will be interesting to further investigate how the SCN cooperates with other brain regions and how the circadian rhythm integrates with homeostatic process.

MATERIALS AND METHODS

Animals

We used CRF-Cre mice (*53*), GAD67-Cre mice (*54*), VGAT-IRES-Cre mice (*55*), Rosa26-LSL-tdTomato mice (the Jackson laboratory, no. 007914), and orexin-flp mice (*24*) on the C57BL/6J background. Mice were bred and reared in the animal facility at the Nagoya University, where environmental conditions were controlled (lights on was 8:00 to 20:00, light intensity was approximately 100 to 300 lux at the bottom of cage, the ambient temperature was 23° ± 2°C, and humidity was 60 ± 10%). Male mice (2 to 5 months) were used in the all experiments, except for locomotor activity, immunohistochemistry, and acute brain slice experiments. All experimental protocols were approved by the Institutional Animal Care and Use Committees, Research Institute of Environmental Medicine, Nagoya University, Japan (approval nos. 18232, 18239, and 18257).

AAV injection in vivo

Mice were anesthetized with isoflurane (induction dose of ~2.5% and maintenance dose of ~1%) and placed in a stereotaxic instrument (David Kopf Instruments). To deliver the AAV into the brain, AAV9-CMV-flex-ChR2-EYFP, AAV9-CMV-flex-hrGFP, AAV9-CMV-flex-hM4Di-mCherry, AAV9-CMV-flex-G-CaMP6, AAV9-CMV-flex-mCherry/DTA, AAV9-CMV-dFRT-tdTomato, AAV9-CMV-hM3Dq-mCherry, or AAV9-CMV-flex-yellowCameleon-Nano50 were injected into the SCN [anteroposterior (AP), ±0.0 mm; mediolateral (ML), ±0.2 mm; dorsoventral (DV), −5.8 mm], the PVN (AP, −0.5 mm; ML, ±0.5 mm; DV, −4.2 mm; for calcium imaging; and AP, −0.4 to 0.5 mm; ML, ±0.2 mm; DV, −4.8 to 4.9 mm; for other experiments), or the LH (AP, −1.4 mm; ML, ±0.8 mm; DV, −5.2 to 5.3 mm) with a glass micropipette and an air pressure injection system (BJ-110, BEX), as previously reported (*9*). One hundred twenty nanoliters of AAV was injected into the SCN, and 600 nl of AAVs was injected into the PVN or LH.

Surgery for EEG/EMG and in vivo optogenetics

Mice were anesthetized with isoflurane, and three screws (U-1430-01; Wilco, Yokohama, Japan) were implanted on the skull for recording of EEG. Two stainless steel wires (AS633; Cooner Wire, Mexico) were also inserted in the rhomboid muscle for recording of EMG. All screws and wires were secured to a connector pin. A fiber-optic cannula [5.0 mm in length, 400-μm-diameter core, and 0.39 numerical aperture (NA); Thorlabs] was stereotaxically implanted just above the PVN (AP, −0.4 to 0.5 mm; ML, ± 0.0 mm; DV, −4.4 to 4.5 mm) or LH (AP, −1.4 mm; ML, ±0.9 mm; DV, −4.8 mm), and it was fixed with dental cement. Carprofen (20 mg/kg; Zoetis Inc., Japan) was administered the day of surgery for its anti-inflammatory and analgesic properties. After surgery, mice were housed separately for at least 7 days for recovery, and then a cable with a slip ring was connected to mice in the cage at least for 5 days before starting of EEG and EMG recordings.

Optogenetic stimulation of CRF neurons in vivo

A flexible fiber-optic cable (M79L005; 400-μm-diameter core and 0.39 NA; Thorlabs) was connected to an optical fiber implanted to CRF-Cre mice, and the cable was attached to an LED (light-emitting diode) light source (Thorlabs; 470 nm, 10 mW at the tip of a fiber). To activate CRF neurons by blue light (frequency, 10 Hz; duration, 10 ms), a pulse generator (SEN 3401; Nihon Kohden, Tokyo, Japan) was connected to an LED driver. The stimulation was performed for 30 s every 15 min for 24 hours. Transistor-transistor-logic (TTL) signals from the pulse generator were also recorded with the EEG and EMG signals to determine the timing of light flashing.

Sleep and wake recordings

EEG and EMG signals were amplified (AB-610J, Nihon Kohden), filtered (EEG, 1.5 to 30 Hz; EMG, 15 to 300 Hz), digitized at a sampling rate of 128 Hz, and recorded using VitalRecorder2 (Kissei Comtec, Nagano, Japan). Animal behavior was recorded by a charge-coupled device (CCD) video camera (SPK-E700CHP1, Keiyo Techno, Japan) and an infrared activity sensor (Biotex, Kyoto, Japan).

Vigilance state determination

EEG and EMG data were automatically scored in 4-s epochs and classified as wakefulness, NREM sleep, or REM sleep by SleepSign3 software (Kissei Comtec), as previously reported (*16*). Wake was

characterized by high EMG amplitude, locomotion score, or low EMG amplitude with low EEG amplitude. NREM sleep was characterized by low EMG amplitude and high EEG δ ($1.5 \leq \delta < 6$ Hz) power, and REM sleep was characterized by low EMG and low EEG amplitude with more than 50% of θ ($6 \leq \theta < 11$ Hz) regular activity. The vigilance state is changed when the successive three epochs show different features of EEG and EMG described above. EEG spectrograms were analyzed using the Signal Processing Toolbox of MATLAB (MathWorks, Natick, MA, USA). Statistics of the probability of vigilance state before and after light stimulation was calculated as follows. We divided four sections in a day (ZT0 to 5, 6 to 11, 12 to 17, and 18 to 23) and calculated the vigilance state every one epoch before and after light stimulation in each animal. Since we applied light stimulation every 15 min, each section has 24 events. Then, we calculated the mean percentage of each vigilance state during each session in each animal (24 events per section) and further calculated the mean percentage of each vigilance state during successive three epochs. We lastly made the mean percentage of successive three epochs in each vigilance state from all animals. Statistics was performed using the mean value obtained from all animals (Figs. 1F and 2G, and figs. S1J and S2G).

Fiber photometry

We used an LED (PlexonBright OPT/LED Blue_TT_FC; Plexon, Dallas, TX) for the light source. The intensity of blue light at the tip of the fiber was 0.07 mW (465 nm). The excitation light was applied through a dichroic mirror and GFP excitation bandpass filter (path, 472 ± 35 nm) and coupled to the silica fiber (NA of 0.39, 400 μm diameter). The G-CaMP6 signals from CRF neurons were collected by the same silica fiber passed through a bandpass emission filter (path, 525 ± 25 nm) and guided to a photomultiplier tube (1P28; Hamamatsu Photonics K.K., Hamamatsu, Japan). G-CaMP6 signals were recorded by VitalRecorder (Kissei Comtec), together with the EEG/EMG signals at a sampling frequency of 128 Hz.

The guide cannula was stereotaxically implanted with a dummy fiber above the PVN more than 2 weeks after AAV injection, and they were fixed to the skull with dental cement. More than 7 days after the surgery, an optical fiber was implanted (AP, +0.4 to 0.5 mm; ML, +0.2 mm; DV, −4.7 mm). Recorded G-CaMP6 signals were smoothed by a 33-point moving average and converted to $\Delta F/F$ (%) as follows: $dF/F = 100*(F(t) - F\min) / F\min$, where $F(t)$ is the G-CaMP6 signal and $F\min$ is the minimum value of the signal. Calcium signals of 1 min before and after stage change were selected and calculated mean value for each animal in Fig. 3. Statistics was performed using mean data obtained from all animals.

Measurement of locomotor activity

Spontaneous movements were measured by a passive infrared sensor that detects changes in animal thermal radiation due to movement (*28*, *56*). Mice were individually housed in a polycarbonate cage placed in a light-tight and air-conditioned box. The amount of movement was recorded every minute with a computer software (ClockLab, Actimetrics).

Inhibition of CRF neurons in the PVN using chemogenetics

AAV9-CMV-flex-hM4Di-mCherry was injected into the PVN of CRF-Cre mice. Two to 3 weeks after AAV injection, EEG electrodes and EMG cables were implanted. One week after that, handling was performed for 3 days, followed by habituation to needle insertion and saline injections (intraperitoneally) for 3 days each. EEG and EMG recordings were then started. Saline or CNO (1.0 mg/kg of body weight) was injected before ZT12. CNO (Enzo Life Sciences, Farmingdale, NY, USA) was dissolved in water as a stock solution (10 mg/ml) and diluted with saline to a final concentration of 100 μg/ml just before use.

Acute brain slice preparation

Acute brain slices were prepared for electrophysiological recordings from male and female mice aged 3 to 5 months at least 3 weeks after AAV microinjection. Animals were deeply anesthetized using isoflurane and decapitated. The brain was then quickly isolated and chilled in an ice-cold cutting solution [110 mM K-gluconate, 15 mM KCl, 0.05 mM EGTA, 5.0 mM Hepes, 26.2 mM $NaHCO_3$, 25 mM glucose, 3.3 mM $MgCl_2$, and 0.0015 mM (±)-3-(2-carboxypiperazin-4-yl) propyl-1-phosphonic acid] gassed with 95% O_2 and 5% CO_2. Coronal brain slices of 300 μm thickness containing either the PVN or LH were cut with a vibratome (VT1200 S; Leica, Wetzlar, Germany) and were temporarily placed in an incubation chamber containing bath solution (124 mM NaCl, 3.0 mM KCl, 2.0 mM $MgCl_2$, 2.0 mM $CaCl_2$, 1.23 mM NaH_2PO_4, 26 mM $NaHCO_3$, and 25 mM glucose) gassed with 95% O_2 and 5% CO_2 in a 35°C water bath for at least 30 min. Slices were then incubated at room temperature in the same incubation chamber for another 30 to 60 min for recovery.

Electrophysiological recording using acute brain slices

Brain slices were transferred into a recording chamber (RC-26G; Warner Instruments, Hamden, CT, USA) on an upright fluorescence microscope (BX51WI; Olympus, Tokyo, Japan) stage. The slices were superfused with 95% O_2 and 5% CO_2 gassed bath solution at the rate of 1.2 ml/min using a peristaltic pump (Dynamax; Rainin, Oakland, CA, USA). An infrared camera (C3077-78; Hamamatsu Photonics, Hamamatsu, Japan) and an electron-multiplying CCD (EMCCD) camera (Evolve 512 delta; Photometrics, Tucson, AZ, USA) were installed with the fluorescence microscope, and both images were separately displayed on monitors. Patch micropipettes of 4- to 6-megohm resistance were prepared from borosilicate glass capillaries (GC150-10; Harvard Apparatus, Cambridge, MA, USA) using a horizontal puller (P-1000; Sutter Instrument, Novato, CA, USA) and were filled with KCl-based internal solution (145 mM KCl, 1.0 mM $MgCl_2$, 10 mM Hepes, 1.1 mM EGTA, 2.0 mM Mg–adenosine 5′-triphosphate, 0.5 mM Na_2–guanosine 5′-triphosphate; pH 7.3 with KOH) with osmolality between 280 and 290 mosm. CRF-positive neurons were identified by the green fluorescence of EYFP, and orexin-positive neurons were identified by red fluorescence of tdTomato. In whole-cell recording, positive pressure was introduced in the patch pipette and a gigaseal of resistance of >1 gigohm was made between the patch pipette and the cell membrane by releasing the positive pressure upon contacting the cell. The patch membrane was then ruptured by gentle suction to make a whole-cell configuration. In loose cell recording, currents were measured without patch membrane rupture. Electrophysiological properties of cells were monitored by the Axopatch 200B amplifier (Axon Instruments, Molecular Devices, Sunnyvale, CA). Output signals were low-pass filtered at 5 kHz and digitized at 10-kHz sampling rate. Patch clamp data were recorded through an analog-to-digital converter (Digidata 1550A, Molecular Devices) using pCLAMP 10.2 software (Molecular Devices). A negative current was injected into the soma of CRF neurons until it stopped spontaneous firing during the current clamp recording to confirm the blue

light–induced action potential. The blue light of 475 ± 17.5 –nm wavelength and 6.9 -mW/mm^2 power was generated by a light source that used an LED (SPECTRA light engine; Lumencor, Beaverton, OR, USA) and was guided to the microscope stage with a 1-cm-diameter optical fiber to illuminate brain slices.

Calcium imaging from the PVN in acute brain slice

A brain slice was transferred into a recording chamber (RC-26G) on an upright fluorescence microscope (BX51WI) stage and superfused with 95% O_2 and 5% CO_2 gassed bath solution with TTX (1 μM; Alomone Labs, Jerusalem, Israel) at the rate of 1.2 ml/min using a peristaltic pump (Dynamax). An EMCCD camera (iXon Ultra 888, Andor, Oxford Instruments, Abingdon, UK), an optical splitter (W-VIEW GEMINI, Hamamatsu Photonics), and a light source (Lumencor) were installed with the microscope. For excitation, blue light (440/40 nm, 150 μW/mm^2, 100 ms) was illuminated. Fluorescent signal of YFP and CFP was monitored in and recorded by MetaFluor 7.8.1 (Molecular Devices). AVP (100 nM), GABA (100 μM), GRP (100 nM), or VIP (100 nM) in bath solution with TTX or only bath solution with TTX (control) were applied for 2 min through perfusion. They were washed out for at least 10 min until calcium signal returned to a baseline. An order of substance application was set at random among experiments (n = 4 animals). Obtained signals of YFP and CFP were motion corrected and aligned by an original program on the basis of scale-invariant feature transform (*57*). Regions of interests (ROIs) were manually created to enclose cell bodies in the corrected images, and the intensity value of YFP and CFP of each ROI was measured by Fiji (*58*). Subsequent calculations were performed in MATLAB (R2019a; MathWorks, Natick, MA, USA). Fluorescence bleaching was corrected as follows: $R_{correct}(t) = R_{raw}(t) + t \times (R_{end} - R_{before}) / (t_{end} - t_{before})$, where t is time from the onset of application of a substance, $R_{correct}(t)$ is corrected Y/C ratio at t, $R_{raw}(t)$ is raw Y/C ratio at t, R_{end} is mean $R_{raw}(t)$ during 2 min before the end of recording, R_{before} is the mean $R_{raw}(t)$ during 2 min before application of a substance, t_{end} is 1 min before the end of recording, and t_{before} is 1 min before application of a substance. Z score was calculated as follows: Z score(t) = $[R_{correct}(t) - \mu]/\sigma$, where Z score($t$) is Z score at t. μ and σ are the means and SD, respectively. Both values were calculated from $R_{correct}(t)$ during 2 min before application of a substance. When the Y/C ratio of CRF neurons was less than −2 (Z score) in consecutive two frames during 3 min after application of a substance, we defined these CRF neurons as suppressed neurons.

Cultured brain slice preparation

Coronal slices (300 μm thick) were made with a tissue chopper (McIlwain) from neonatal mice at postnatal days 6 to 8, and the SCN-PVN area was dissected at the mid–rostro-caudal region. A paired SCN-PVN was cultured on a Millicell-CM culture insert (Millipore Corporation), as described previously (*59*). Briefly, the slice was cultured at 36.5°C with 1.0 ml of Dulbecco's modified Eagle's medium (Invitrogen) with 0.1 mM D-luciferin K and 5% fetal bovine serum. Two to 4 days after that, AAV were inoculated onto the surface of the cultured brain slice. More than 18 days after infection of AAV, calcium recording was started.

Bioluminescent Ca^{2+} indicator gene construction

Complementary DNA of firefly luciferase derived from *Pyrocoelia matsumurai* (Oki) and *Stenocladius flavipennis* (SfRE) were gifts from K. Ogo (Olympus Corporation). To construct Okiluc-CaM, the N terminal of a calmodulin-M13 fragment of cameleon, a genetically encoded Ca^{2+} indicator, was fused to the C-terminal half (residues T352 to M555) of SfRE luciferase, and the C terminal of the fragment was fused to the N-terminal half (residues M1 to D416) of Oki luciferase. For bacterial expression, the *Okiluc-CaM* gene was subcloned into the Bam HI/Eco RI sites of pRSET-B to construct pRSET-Okiluc-CaM.

In vitro titration of bioluminescent indicators

Recombinant proteins were purified from bacteria transformed with the pRSET-Okiluc-CaM plasmid using QIAexpressionist (Qiagen), following the manufacturer's instructions. The concentration of purified protein was determined using Bio-Rad Protein Assay and diluted with a buffer consisting of 10 mM EGTA, 100 mM KCl, and 10 mM Mops (pH 7.2) to the concentration of 1 μg of protein per microliter. Ca^{2+} titration was performed using a Ca^{2+} calibration buffer kit (Invitrogen), according to the manufacturer's manual. Briefly, 1 μg of recombinant protein was added to 50 μl of Ca^{2+} buffer and incubated for 10 min at room temperature (23 to 24°C). Following incubation, 50 μl of sample was added to 50 μl of the Luciferase Assay Reagent (Bright-Glo, Promega) solution and incubated further for 15 min at room temperature. Luminescence was measured using Luminescencer JNR (ATTO Corporation, Tokyo, Japan). The averaged data from four independent measurements were fitted using Microsoft Excel 2003, and the results are expressed as means ± SD.

Calcium imaging from the cultured brain slice

Petri dishes containing cultured brain slices were placed in a mini-incubator installed on the stage of a microscope (ECRIPSE-NiU, Nikon) equipped with an EMCCD camera (ImagEM, Hamamatsu Photonics). Fluorescent calcium sensor (GCaMP6s) was excited (470/40 nm) with an LED light source (X-Cite 120, Excelitas) and visualized with 500-nm dichroic mirror and 535/50-nm emission filters (SemLock), as previously reported (*60*). GCaMP6s signals were measured every 1 s with 400-ms exposure (470 nm, 0.4 μW/mm^2). Bioluminescence from the SCN-PVN slice was measured every 30 s with an exposure time of 29 s. Imaging data were analyzed by ImageJ.

Optical stimulation and recording in the cultured brain slice

Petri dishes containing cultured brain slices were placed in an LED array system (590 nm; LEDA-Y, BRC Bio Research Center) within in a mini-incubator installed on the stage of a microscope. To deliver the AAV into the brain slice, 500 to 800 nl of AAV9-CMV-flex-SSFO-mCherry and AAV9-hSyn-Okiluc-CaM or AAV9-hSyn-GCaMP6s and AAV9-CAG-flex-ChrimsonR-tdTomato was inoculated onto the surface of the slice. When the optical stimulation by ChrimsonR was performed, GCaMP6s signals were measured every 1 s with 400-ms exposure (0.4 μW/mm^2) followed by 50-ms dead time, 500-ms excitation (590 nm, 0.063 mW/mm^2) of ChrimsonR, and 50-ms dead time. Timing of recording and stimulation was regulated by TTL signal generated by a stimulator (STOmk-2, BRC Bio Research Center). When the optical stimulation by SSFO was performed, continuous blue light (0.2 mm W/mm^2) for 5 s was applied.

Histological study

Mice were anesthetized with isoflurane and perfused with saline followed by a 10% formalin solution (Wako). Brains were extracted

and postfixed in the same solution for 24 hours at 4°C, followed by a 30% sucrose solution at 4°C for at least 2 days. Thirty- or 40-μm coronal sections of the SCN were made using a cryostat (Leica CM3050S; Leica Microsystems, Wetzlar, Germany) and stored at 4°C in phosphate-buffered saline (PBS). Immunostaining was performed, as previously described (*9*). Brain sections were immersed in blocking buffer (1% bovine serum albumin and 0.25% Triton X-100 in PBS) and then incubated with primary antibodies at 4°C overnight. The sections were washed with blocking buffer and then incubated with secondary antibodies at 4°C overnight. The brain sections were mounted and examined with a fluorescence microscope (BZ-9000, Keyence) or a confocal microscope (LSM710; Carl Zeiss, Oberkochen, Germany). Primary and secondary antibodies were diluted in blocking buffer as follows: anti–c-Fos rabbit antibody (Santa Cruz Biotechnology Inc., Dallas, TX, USA) at 1:500, anti–orexin-A goat antibody (Santa Cruz Biotechnology Inc.) at 1:1000, anti-GFP mouse antibody (Wako Pure Chemical Industries) at 1:1000, anti-CRF rabbit antibody (HAC-HM04-01RBP90, Gunma University) at 1:1000, CF 488–conjugated anti-mouse or anti-rabbit (Biotium Inc., Hayward, CA, USA) at 1:1000, and CF 594–conjugated anti-rabbit or anti-goat antibody (Biotium) at 1:1000. For cell counting, a series consisting of every fourth brain section containing the PVN, and other regions was examined with a fluorescence microscope. Cell counting was performed by using ImageJ.

Statistics

Statistical analyses were performed using R, Statview, or Statcel 3.

SUPPLEMENTARY MATERIALS

Supplementary material for this article is available at http://advances.sciencemag.org/cgi/content/full/6/45/eabd0384/DC1

View/request a protocol for this paper from *Bio-protocol*.

REFERENCES AND NOTES

1. J. Bass, J. S. Takahashi, Circadian integration of metabolism and energetics. *Science* **330**, 1349–1354 (2010).
2. D. K. Welsh, D. E. Logothetis, M. Meister, S. M. Reppert, Individual neurons dissociated from rat suprachiasmatic nucleus express independently phased circadian firing rhythms. *Neuron* **14**, 697–706 (1995).
3. S. Yamaguchi, H. Isejima, T. Matsuo, R. Okura, K. Yagita, M. Kobayashi, H. Okamura, Synchronization of cellular clocks in the suprachiasmatic nucleus. *Science* **302**, 1408–1412 (2003).
4. S. M. Reppert, D. R. Weaver, Coordination of circadian timing in mammals. *Nature* **418**, 935–941 (2002).
5. R. Y. Moore, N. J. Lenn, A retinohypothalamic projection in the rat. *J. Comp. Neurol.* **146**, 1–14 (1972).
6. F. K. Stephan, I. Zucker, Circadian rhythms in drinking behavior and locomotor activity of rats are eliminated by hypothalamic lesions. *Proc. Natl. Acad. Sci. U.S.A.* **69**, 1583–1586 (1972).
7. S. T. Inouye, H. Kawamura, Persistence of circadian rhythmicity in a mammalian hypothalamic "island"s containing the suprachiasmatic nucleus. *Proc. Natl. Acad. Sci. U.S.A.* **76**, 5962–5966 (1979).
8. R. Y. Moore, J. C. Speh, GABA is the principal neurotransmitter of the circadian system. *Neurosci. Lett.* **150**, 112–116 (1993).
9. D. Ono, K.-i. Honma, Y. Yanagawa, A. Yamanaka, S. Honma, GABA in the suprachiasmatic nucleus refines circadian output rhythms in mice. *Commun. Biol.* **2**, 232 (2019).
10. Y. Oishi, Q. Xu, L. Wang, B.-J. Zhang, K. Takahashi, Y. Takata, Y.-J. Luo, Y. Cherasse, S. N. Schiffmann, A. de Kerchove d'Exaerde, Y. Urade, W.-M. Qu, Z.-L. Huang, M. Lazarus, Slow-wave sleep is controlled by a subset of nucleus accumbens core neurons in mice. *Nat. Commun.* **8**, 734 (2017).
11. C. Anaclet, L. Ferrari, E. Arrigoni, C. E. Bass, C. B. Saper, J. Lu, P. M. Fuller, The GABAergic parafacial zone is a medullary slow wave sleep–promoting center. *Nat. Neurosci.* **17**, 1217–1224 (2014).
12. X. Yu, W. Li, Y. Ma, K. Tossell, J. J. Harris, E. C. Harding, W. Ba, G. Miracca, D. Wang, L. Li, J. Guo, M. Chen, Y. Li, R. Yustos, A. L. Vyssotski, D. Burdakov, Q. Yang, H. Dong, N. P. Franks, W. Wisden, GABA and glutamate neurons in the VTA regulate sleep and wakefulness. *Nat. Neurosci.* **22**, 106–119 (2019).
13. S. Chung, F. Weber, P. Zhong, C. L. Tan, T. N. Nguyen, K. T. Beier, N. Hörmann, W.-C. Chang, Z. Zhang, J. P. Do, S. Yao, M. J. Krashes, B. Tasic, A. Cetin, H. Zeng, Z. A. Knight, L. Luo, Y. Dan, Identification of preoptic sleep neurons using retrograde labelling and gene profiling. *Nature* **545**, 477–481 (2017).
14. C. B. Saper, T. E. Scammell, J. Lu, Hypothalamic regulation of sleep and circadian rhythms. *Nature* **437**, 1257–1263 (2005).
15. A. R. Adamantidis, F. Zhang, A. M. Aravanis, K. Deisseroth, L. de Lecea, Neural substrates of awakening probed with optogenetic control of hypocretin neurons. *Nature* **450**, 420–424 (2007).
16. T. Tsunematsu, T. S. Kilduff, E. S. Boyden, S. Takahashi, M. Tominaga, A. Yamanaka, Acute optogenetic silencing of orexin/hypocretin neurons induces slow-wave sleep in mice. *J. Neurosci.* **31**, 10529–10539 (2011).
17. R. K. Leak, R. Y. Moore, Topographic organization of suprachiasmatic nucleus projection neurons. *J. Comp. Neurol.* **433**, 312–334 (2001).
18. A. G. Watts, L. W. Swanson, Efferent projections of the suprachiasmatic nucleus: II. Studies using retrograde transport of fluorescent dyes and simultaneous peptide immunohistochemistry in the rat. *J. Comp. Neurol.* **258**, 230–252 (1987).
19. A. G. Watts, L. W. Swanson, G. Sanchez-Watts, Efferent projections of the suprachiasmatic nucleus: I. Studies using anterograde transport of Phaseolus vulgaris leucoagglutinin in the rat. *J. Comp. Neurol.* **258**, 204–229 (1987).
20. E. E. Abrahamson, R. Y. Moore, Suprachiasmatic nucleus in the mouse: Retinal innervation, intrinsic organization and efferent projections. *Brain Res.* **916**, 172–191 (2001).
21. R. E. Sutton, G. F. Koob, M. Le Moal, J. Rivier, W. Vale, Corticotropin releasing factor produces behavioural activation in rats. *Nature* **297**, 331–333 (1982).
22. T. Tsunematsu, T. Ueno, S. Tabuchi, A. Inutsuka, K. F. Tanaka, H. Hasuwa, T. S. Kilduff, A. Terao, A. Yamanaka, Optogenetic manipulation of activity and temporally controlled cell-specific ablation reveal a role for MCH neurons in sleep/wake regulation. *J. Neurosci.* **34**, 6896–6909 (2014).
23. R. M. Chemelli, J. T. Willie, C. M. Sinton, J. K. Elmquist, T. Scammell, C. Lee, J. A. Richardson, S.-C. Williams, Y. Xiong, Y. Kisanuki, T. E. Fitch, M. Nakazato, R. E. Hammer, C. B. Saper, M. Yanagisawa, Narcolepsy in *orexin* knockout mice: Molecular genetics of sleep regulation. *Cell* **98**, 437–451 (1999).
24. S. Chowdhury, C. J. Hung, S. Izawa, A. Inutsuka, M. Kawamura, T. Kawashima, H. Bito, I. Imayoshi, M. Abe, K. Sakimura, A. Yamanaka, Dissociating orexin-dependent and -independent functions of orexin neurons using novel Orexin-Flp knock-in mice. *eLife* **8**, e44927 (2019).
25. Y. C. Saito, T. Maejima, M. Nishitani, E. Hasegawa, Y. Yanagawa, M. Mieda, T. Sakurai, Monoamines inhibit GABAergic neurons in ventrolateral preoptic area that make direct synaptic connections to hypothalamic arousal neurons. *J. Neurosci.* **38**, 6366–6378 (2018).
26. M. Ohkura, T. Sasaki, J. Sadakari, K. Gengyo-Ando, Y. Kagawa-Nagamura, C. Kobayashi, Y. Ikegaya, J. Nakai, Genetically encoded green fluorescent Ca^{2+} indicators with improved detectability for neuronal Ca^{2+} signals. *PLOS ONE* **7**, e51286 (2012).
27. J. Kim, S. Lee, Y.-Y. Fang, A. Shin, S. Park, K. Hashikawa, S. Bhat, D. Kim, J.-W. Sohn, D. Lin, G. S. B. Suh, Rapid, biphasic CRF neuronal responses encode positive and negative valence. *Nat. Neurosci.* **22**, 576–585 (2019).
28. H. Abe, S. Honma, H. Ohtsu, K.-i. Honma, Circadian rhythms in behavior and clock gene expressions in the brain of mice lacking histidine decarboxylase. *Brain Res. Mol. Brain Res.* **124**, 178–187 (2004).
29. K. Horikawa, Y. Yamada, T. Matsuda, K. Kobayashi, M. Hashimoto, T. Matsu-ura, A. Miyawaki, T. Michikawa, K. Mikoshiba, T. Nagai, Spontaneous network activity visualized by ultrasensitive Ca^{2+} indicators, yellow Cameleon-Nano. *Nat. Methods* **7**, 729–732 (2010).
30. N. Inagaki, S. Honma, D. Ono, Y. Tanahashi, K.-i. Honma, Separate oscillating cell groups in mouse suprachiasmatic nucleus couple photoperiodically to the onset and end of daily activity. *Proc. Natl. Acad. Sci. U.S.A.* **104**, 7664–7669 (2007).
31. A. Kalsbeek, M.-L. Garidou, I. F. Palm, J. van der Vliet, V. Simonneaux, P. Pévet, R. M. Buijs, Melatonin sees the light: Blocking GABA-ergic transmission in the paraventricular nucleus induces daytime secretion of melatonin. *Eur. J. Neurosci.* **12**, 3146–3154 (2000).
32. R. A. Hoffman, R. J. Reiter, Pineal gland: Influence on gonads of male hamsters. *Science* **148**, 1609–1611 (1965).
33. S. Amir, Stimulation of the paraventricular nucleus with glutamate activates interscapular brown adipose tissue thermogenesis in rats. *Brain Res.* **508**, 152–155 (1990).
34. D. Atasoy, J. N. Betley, H. H. Su, S. M. Sternson, Deconstruction of a neural circuit for hunger. *Nature* **488**, 172–177 (2012).
35. A. Balsalobre, S. A. Brown, L. Marcacci, F. Tronche, C. Kellendonk, H. M. Reichardt, G. Schütz, U. Schibler, Resetting of circadian time in peripheral tissues by glucocorticoid signaling. *Science* **289**, 2344–2347 (2000).

36. Y. M. Ulrich-Lai, J. P. Herman, Neural regulation of endocrine and autonomic stress responses. *Nat. Rev. Neurosci.* **10**, 397–409 (2009).
37. Y. Yuan, W. Wu, M. Chen, F. Cai, C. Fan, W. Shen, W. Sun, J. Hu, Reward inhibits paraventricular CRH neurons to relieve stress. *Curr. Biol.* **29**, 1243–1251.e4 (2019).
38. A. Venner, C. Anaclet, R. Y. Broadhurst, C. B. Saper, P. M. Fuller, A novel population of wake-promoting GABAergic neurons in the ventral lateral hypothalamus. *Curr. Biol.* **26**, 2137–2143 (2016).
39. I. Gvilia, N. Suntsova, S. Kumar, D. McGinty, R. Szymusiak, Suppression of preoptic sleep-regulatory neuronal activity during corticotropin-releasing factor-induced sleep disturbance. *Am. J. Physiol. Regul. Integr. Comp. Physiol.* **309**, R1092–R1100 (2015).
40. I. Gvilia, S. Kumar, D. McGinty, R. Szymusiak, The effect of chemogenetic silencing of corticotropin releasing factor neurons in the paraventricular nucleus on post-stress sleep in mice. *Sleep* **42**, A2 (2019).
41. M. P. Butler, M. N. Rainbow, E. Rodriguez, S. M. Lyon, R. Silver, Twelve-hour days in the brain and behavior of split hamsters. *Eur. J. Neurosci.* **36**, 2556–2566 (2012).
42. C. Gizowski, C. Zaelzer, C. W. Bourque, Clock-driven vasopressin neurotransmission mediates anticipatory thirst prior to sleep. *Nature* **537**, 685–688 (2016).
43. S. Paul, L. Hanna, C. Harding, E. A. Hayter, L. Walmsley, D. A. Bechtold, T. M. Brown, Output from VIP cells of the mammalian central clock regulates daily physiological rhythms. *Nat. Commun.* **11**, 1453 (2020).
44. S. Ren, Y. Wang, F. Yue, X. Cheng, R. Dang, Q. Qiao, X. Sun, X. Li, Q. Jiang, J. Yao, H. Qin, G. Wang, X. Liao, D. Gao, J. Xia, J. Zhang, B. Hu, J. Yan, Y. Wang, M. Xu, Y. Han, X. Tang, X. Chen, C. He, Z. Hu, The paraventricular thalamus is a critical thalamic area for wakefulness. *Science* **362**, 429–434 (2018).
45. X. Yu, Z. Ye, C. M. Houston, A. Y. Zecharia, Y. Ma, Z. Zhang, D. S. Uygun, S. Parker, A. L. Vyssotski, R. Yustos, N. P. Franks, S. G. Brickley, W. Wisden, Wakefulness is governed by GABA and histamine cotransmission. *Neuron* **87**, 164–178 (2015).
46. J. Lu, M. A. Greco, P. Shiromani, C. B. Saper, Effect of lesions of the ventrolateral preoptic nucleus on NREM and REM sleep. *J. Neurosci.* **20**, 3830–3842 (2000).
47. C. S. Pittendrigh, S. Daan, A functional analysis of circadian pacemakers in nocturnal rodents. V. Pacemaker structure: Clock for all seasons. *J. Comp. Physiol.* **106**, 333–355 (1976).
48. D. Stoleru, Y. Peng, J. Agosto, M. Rosbash, Coupled oscillators control morning and evening locomotor behaviour of *Drosophila*. *Nature* **431**, 862–868 (2004).
49. T. Sato, H. Kawamura, Circadian rhythms in multiple unit activity inside and outside the suprachiasmatic nucleus in the diurnal chipmunk (*Eutamias sibiricus)*. *Neurosci. Res.* **1**, 45–52 (1984).
50. Y. Ben-Ari, Excitatory actions of gaba during development: The nature of the nurture. *Nat. Rev. Neurosci.* **3**, 728–739 (2002).
51. Z. Wang, J. Ma, C. Miyoshi, Y. Li, M. Sato, Y. Ogawa, T. Lou, C. Ma, X. Gao, C. Lee, T. Fujiyama, X. Yang, S. Zhou, N. Hotta-Hirashima, D. Klewe-Nebenius, A. Ikkyu, M. Kakizaki, S. Kanno, L. Cao, S. Takahashi, J. Peng, Y. Yu, H. Funato, M. Yanagisawa, Q. Liu, Quantitative phosphoproteomic analysis of the molecular substrates of sleep need. *Nature* **558**, 435–439 (2018).
52. F. Tatsuki, G. A. Sunagawa, S. Shi, E. A. Susaki, H. Yukinaga, D. Perrin, K. Sumiyama, M. Ukai-Tadenuma, H. Fujishima, R.-i. Ohno, D. Tone, K. L. Ode, K. Matsumoto, H. R. Ueda, Involvement of Ca^{2+}-dependent hyperpolarization in sleep duration in mammals. *Neuron* **90**, 70–85 (2016).
53. K. Itoi, A. H. Talukder, T. Fuse, T. Kaneko, R. Ozawa, T. Sato, T. Sugaya, K. Uchida, M. Yamazaki, M. Abe, R. Natsume, K. Sakimura, Visualization of corticotropin-releasing factor neurons by fluorescent proteins in the mouse brain and characterization of labeled neurons in the paraventricular nucleus of the hypothalamus. *Endocrinology* **155**, 4054–4060 (2014).
54. S. Wu, S. Esumi, K. Watanabe, J. Chen, K. C. Nakamura, K. Nakamura, K. Kometani, N. Minato, Y. Yanagawa, K. Akashi, K. Sakimura, T. Kaneko, N. Tamamaki, Tangential migration and proliferation of intermediate progenitors of GABAergic neurons in the mouse telencephalon. *Development* **138**, 2499–2509 (2011).
55. L. Vong, C. Ye, Z. Yang, B. Choi, S. Chua Jr., B. B. Lowell, Leptin action on GABAergic neurons prevents obesity and reduces inhibitory tone to POMC neurons. *Neuron* **71**, 142–154 (2011).
56. D. Ono, S. Honma, K.-i. Honma, Differential roles of AVP and VIP signaling in the postnatal changes of neural networks for coherent circadian rhythms in the SCN. *Sci. Adv.* **2**, e1600960 (2016).
57. D. G. Lowe, Distinctive image features from scale-invariant keypoints. *Int. J. Comput. Vis.* **60**, 91–110 (2004).
58. J. Schindelin, I. Arganda-Carreras, E. Frise, V. Kaynig, M. Longair, T. Pietzsch, S. Preibisch, C. Rueden, S. Saalfeld, B. Schmid, J.-Y. Tinevez, D. J. White, V. Hartenstein, K. Eliceiri, P. Tomancak, A. Cardona, Fiji: An open-source platform for biological-image analysis. *Nat. Methods* **9**, 676–682 (2012).
59. D. Ono, S. Honma, K.-i. Honma, *Cryptochromes* are critical for the development of coherent circadian rhythms in the mouse suprachiasmatic nucleus. *Nat. Commun.* **4**, 1666 (2013).
60. D. Ono, S. Honma, Y. Nakajima, S. Kuroda, R. Enoki, K.-i. Honma, Dissociation of *Per1* and *Bmal1* circadian rhythms in the suprachiasmatic nucleus in parallel with behavioral outputs. *Proc. Natl. Acad. Sci. U.S.A.* **114**, E3699–E3708 (2017).

Acknowledgments: We thank M. P. Butler for the valuable discussion of this study; S. Honma, K. Honma, Y. Yamanaka, T. Yoshimura, and N. Hayasaka for the technical advice; G. Wang for the supporting analysis; and Y. Miyoshi, S. Tsukamoto, and S. Nasu for the animal care. We also thank the Institute for Molecular and Cellular Regulation for providing CRF antibody (HAC-HM04-01RBP90), B. Lowell for providing Vgat-IRES-Cre mice, K. Itoi for providing CRF-Cre mice, H. Bito for the providing dFRT sequence, the Genetically-Encoded Neuronal Indicator and Effector Project and the Janelia Farm Research Campus of the Howard Hughes Medical Institute for sharing GCaMP6s constructs, M. Ohkura for providing G-CaMP6 plasmid, and T. Nagai for providing the Yellow Camelon-Nano50 plasmid. **Funding:** This work was supported by The Uehara Memorial Foundation, Kowa Life Science Foundation, Takeda Science Foundation, Kato Memorial Bioscience Foundation, DAIKO FOUNDATION, SECOM Science and Technology Foundation, Research Foundation for Opto-Science and Technology, The Nakatani Foundation for Advancement of Measuring Technologies in Biomedical Engineering, JST CREST (JPMJCR1656 to A.Y.), and the JSPS KAKENHI (18H02477 to D.O., 18J21665 to Y.M., and 20H05061, 19H05016, 18H02523, and 18KK0223 to A.Y). **Author contribution:** D.O. designed the study; D.O., Y.M., C.J.H., and S.C. performed experiments; D.O., Y.M., C.J.H., and S.C. contributed to the analysis; T.S. made the bioluminescence probe; and A.Y. and D.O. discussed the research and wrote the manuscript. **Competing interests:** The authors declare that they have no competing interests. **Data and materials availability:** The SSFO, ChrimsonR, and hM4Di expression plasmid can be provided by K. Deisseroth, E. Boyden, and B. Roth, respectively, pending scientific review and a completed material transfer agreement. Requests for the plasmids should be submitted to: K. Deisseroth, E. Boyden, or B. Roth. All data needed to evaluate the conclusions in the paper are present in the paper and/or the Supplementary Materials. Additional data related to this paper may be requested from the authors.

Submitted 27 May 2020
Accepted 23 September 2020
Published 6 November 2020
10.1126/sciadv.abd0384

Citation: D. Ono, Y. Mukai, C. J. Hung, S. Chowdhury, T. Sugiyama, A. Yamanaka, The mammalian circadian pacemaker regulates wakefulness via CRF neurons in the paraventricular nucleus of the hypothalamus. *Sci. Adv.* **6**, eabd0384 (2020).